IEEE Access
Multidisciplinary ⋮ Rapid Review ⋮ Open Access Journal

Received April 11, 2022, accepted April 27, 2022, date of publication May 2, 2022, date of current version June 3, 2022.

Digital Object Identifier 10.1109/ACCESS.2022.3171581

Design and Analysis of a Magnetic Field Communication System Using a Giant Magneto-Impedance Sensor

SEUNGHUN RYU[1], KIBEOM KIM[1], JANG-YEOL KIM[2], IN-KUI CHO[2], HAERIM KIM[1], JANGYONG AHN[1], JUNSUNG CHOI[3], (Member, IEEE), AND SEUNGYOUNG AHN[1], (Senior Member, IEEE)

[1]The Cho Chun Shik Graduate School of Green Transportation, Korea Advanced Institute of Science and Technology, Daejeon 34051, South Korea
[2]Radio & Satellite Research Division, Electronics and Telecommunications Research Institute, Daejeon 34129, South Korea
[3]Center for Green Transportation System, Korea Advanced Institute of Science and Technology, Daejeon 34051, South Korea

Corresponding authors: Seungyoung Ahn (sahn@kaist.ac.kr) and Junsung Choi (choijs89@kaist.ac.kr)

This work was supported by the Institute of Information & Communications Technology Planning & Evaluation (IITP) funded by the Korean Government [Ministry of Science and ICT (MSIT)] through the Magnetic Field Communication Technology Based on 10pT Class Magnetic Field for Middle and Long Range under Grant 2019-0-00007.

ABSTRACT Given the interest of researchers for wireless communications in electromagnetic (EM) shadow areas, a magnetic field communication has emerged to overcome RF challenges based on magnetic permeability characteristics. However, magnetic field communication has the demerit of a short communication range. Considering this limitation, we have proposed the GMI sensor-based field receiver to obtain immunity to low-frequency noise and high sensitivity for extension of communication range in previous studies. Further, this paper designs a magnetic field communication system with a GMI sensor-based receiver including a transmitter. Even though the basic concept of magnetic field communication is taken from previous studies, this study conducts the different realization of the system with transmitter system and communication link. Besides, this paper proposes the experiment of magnetic field communication using a GMI sensor-based system to verify its applicability in the practical environment for the first time. Bit error rate (BER), spurious-free dynamic range (SFDR), and random noise are measured with an on-off keying (OOK) communication link to analyze the stability and reliability of the system. The experimental verification and analysis entail the conditions of communication distance and channel medium to mimic practical communication in atmospheric, underwater, and underground environments. A comprehensive analysis of the system design and experimental verification for application in a practical environment show the possibility of the proposed system to realize improved wireless communications in EM shadow areas.

INDEX TERMS Giant magneto impedance (GMI), magnetic field communication, magnetic field path loss (MFPL), spurious-free dynamic range (SFDR), random noise.

I. INTRODUCTION

The demand for wireless communications in electromagnetic (EM) shadow areas, such as underwater and underground environments, continues to increase. Wireless sensor networks (WSNs) are representative examples of communications in this area. WSNs provide opportunities to administrate underground facilities such as power lines and pipelines and to monitor water pollution and natural disasters in an underwater environment. The conventional communication technique that adopts EM waves encounters many RF challenges, such as multipath fading, and high attenuation in the underwater and underground medium. Such challenges result in an increase in the BER and a decrease in the communication range.

Magnetic fields have been proposed as an alternative data carrier instead of EM waves to overcome these communication issues. Magnetic fields operate in the near field and are largely dominated by magnetic permeability with regard to penetration into materials. Because most materials, except for ferromagnetic materials, have the same permeability of 1 which is identical to the one of air, a magnetic field can

The associate editor coordinating the review of this manuscript and approving it for publication was Barbara Masini.

travel through materials without signal distortion. Hence, magnetic field signals are free from RF challenges generated in the EM shadow area. Because magnetic fields form in the near-field region, communications dealing with magnetic fields operate at a lower frequency than the frequency band of the EM wave signal. Low-frequency features contribute to low attenuation of the signals because the lower frequency is linked to a lower skin effect. However, the low frequency means a low data rate of the communication system. Considering the purpose of magnetic field communications, such as the monitoring function which does not need high-speed signaling, the relatively low data rates of the magnetic field signaling can be adopted in the system. The most typical method of magnetic field communication is magnetic induction (MI), which uses loop coils as the antenna of the transmitter and receiver to induce the magnetic field and the voltage signal. MI-based communication utilizes the magnetic field as the signal carrier and uses a loop antenna as the transmitter and receiver to induce the magnetic field.

However, MI-based communication has the issue with the constraint of a short communication range. This is due to the low sensitivity of the loop antenna on a confined scale. Increasing the number of turns and the size of the coils can improve the sensitivity; however, these strategies cause an increase in the volume of the receiver system and incur additional costs. Therefore, various studies to extend the communication range by improving the receiver sensitivity have been conducted. Resonant coils are utilized to transmit the magnetic signal effectively based on a high quality factor [1]. Also, a gaped two-loop antenna with the space of the antenna radius optimized for energy efficiency has been proposed [2]. This study shows that MI-based data links over 25m can be utilized when the power of the transmitter exceeds 30dBm. Moreover, some researchers have introduced a relay coil as the MI waveguide between the transmitter and receiver system [3]. With this technique, a reduction of path loss can be achieved, and the communication range can be extended. Research adopting a magnetic sensor as a receiver has also been conducted in an effort to realize high-performance of magnetic field reception. [4] proposed the optically pumped magnetometer (OPM)-based communication system using a binary phase shift keying (BPSK) modulation. The experimental verification was conducted with the identification of the detected signal in the time and frequency domain. The anisotropic magneto-resistive (AMR) sensor is adopted to receive the magnetic field signal in [5], [6]. [5] estimated the communication range of the system based on the calculation. [6] proposed the AMR sensor-based communication system with a small-scale prototype and theoretical analysis.

The receiver adopts a giant magneto-impedance (GMI) sensor as a possible solution to overcome the short communication range [7], [8]. It should be noted that the principle of detecting an external magnetic field is the GMI effect, which is totally different from the conventional MI. The GMI effect, which is the principle of the GMI sensor, is defined as a phenomenon by which the impedance of a ferromagnetic wire changes largely due to an external magnetic field parallel to the direction of the wire. The higher impedance increased by the external magnetic field results in the higher output voltage of the sensor according to the presence of a driving current. In other words, a wide variation of the impedance leads to a high magnetic field-to-voltage conversion ratio (MVCR) and high sensitivity. The sensitivity of the GMI sensor is introduced as the pico-tesla level in [9]. The OPM sensor and superconducting quantum interference device (SQUID) sensor have much better sensitivity than the GMI sensor; however, they have technical issues with the operating condition and portability. The OPM sensor should be shielded and cancel the residual field to sustain due to the vulnerability to interference [10]. The SQUID sensor also needs to be shielded. Furthermore, this sensor relies on the cooling of the sensing element with liquid nitrogen or helium. It results in an increase of the system volume and cost. Accordingly, the OPM and SQUID sensors are difficult to apply to the practical system and are minimized because of the peripheral to support the sensor operation. Except for the OPM and SQUID sensor, there are AMR, GMR, Hall effect, and magneto-optical sensors as the magnetic field receiver. AMR and GMR sensors have sensitivity to the level of nano-tesla. In the case of the Hall effect and magneto-optical sensor, they are on the micro-tesla level. Even though four of the sensor can be operated in the form of small-sized and integrated, they are worse than the GMI sensor in terms of sensitivity. In conclusion, the GMI sensor can be considered the best sensor to utilize in the practical magnetic field communication system [5], [9], [11].

Moreover, the GMI sensor has the unique characteristic of a superheterodyne radio topology, which facilitates amplitude modulation (AM) with an external magnetic field. This feature can be greatly advantageous for communication using frequencies in the range of several hundreds of kilohertz. The low-frequency environment generates flicker (1/f) noise on a receiver; however, the superheterodyne topology raises the frequency of the voltage signal. Therefore, the flicker noise becomes negligible in the GMI sensor. This topology upconverts the frequency band of the external magnetic field to the upper band, where low-frequency noise cannot affect the signal reception. Therefore, the background noise composed of low-frequency components can be overcome by the superheterodyne topology of the GMI sensor.

We studied the possibility of the GMI sensor as the receiver for magnetic field signals in a wireless communication system [7]. We presented a comprehensive analysis of the GMI sensor, examining the bandwidth, noise spectral density, and channel capacity with two types of GMI sensors to verify their applicability in magnetic field communications. The bandwidth of the GMI sensor at 50 to 70kHz was sustained at a level near 20 kHz. This shows the feasibility of achieving the data rate of kbps. In the case of channel capacity, the GMI sensor achieved the capacity of over 300kbps at 50 to 70kHz. This figure is enough to cover the voice data and shows the applicability of the sensor to the various communication

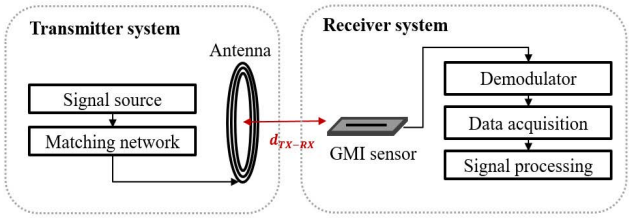

FIGURE 1. Concept of the proposed communication system using a magnetic field link.

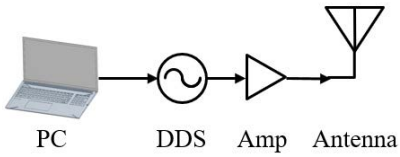

FIGURE 2. Schematic of the transmitter system composed of a PC, DDS, amplifier and resonant antenna.

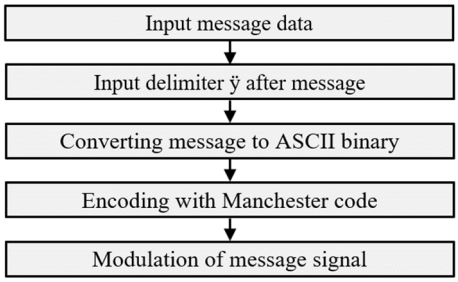

FIGURE 3. Flow chart of signal generation in a PC and DDS.

device. Moreover, the noise spectral density is measured to 1.5 $pT/\sqrt{Hz}$ at 20.03 MHz, and 3 $pT/\sqrt{Hz}$ at 3MHz. Subsequently, we studied the characteristics of the GMI sensor in a receiver system [8]. The MVCR, spurious-free dynamic range (SFDR) from the output of the sensor and the receiver sensitivity were measured to confirm the feasibility of magnetic field communication in the practical system. The experiment was conducted with Helmholtz coils generating a uniform magnetic field and the GMI sensor located between the coils at set distances of 10cm. The message signal in the form of binary ASCII code could be identified through the receiver system.

In this paper, we design the magnetic field communication system, including the GMI sensor-based receiver and transmitter with a loop antenna. A comprehensive analysis of the whole system from transmitter to receiver is proposed first. Furthermore, the experimental verification of the system is proposed and analyzed to identify the applicability in the practical environment. The BER, SFDR, and random noise as the communication performance metrics are measured in the experiment with the additional conditions of communication distance and channel media to mimic the atmospheric, underwater, and underground environments. The measurement results, according to the attenuation with distance and electrical conductivity change with channel media, show the applicability of the GMI sensor-based magnetic field communication to practical EM shadow area. This experimental verification for the GMI sensor-based communication system is proposed for the first time. This study can give insight into advanced communication systems and introduce further works of the GMI sensor-based communication system.

The outline of the paper is as follows. Section II shows the system overview, including the transmitter and receiver, through a schematic and a description of the function of each component. Also, the signal processing algorithm, which handles decoding and demodulating the message signal, is described in detail. Section III presents the analysis and evaluation of the magnetic field channel. In this section, magnetic field path loss of the channel is calculated, and the communication distance is estimated through the sensitivity of the sensor. Section IV shows the measurement scenarios, including the method and environments of the measurements and design parameters listed. Section V shows the results of a comprehensive communication performance analysis in terms of the BER, SFDR, and random noise. The paper is concluded in Section VI.

II. SYSTEM OVERVIEW

This section describes the structure and functions of the full communication system, including the transmitter and receiver. The process of communication is shown in Figure 1. A direct digital synthesizer (DDS) forms a voltage signal, which is encoded and modulated with on-off keying (OOK). The voltage signal is converted into a magnetic field signal and transmitted to the receiver. The message signal is received by the GMI sensor and demodulated in the following circuit and sent to a PC as a digital binary signal for decoding of the signal.

A. TRANSMITTER SYSTEM

The transmitter system consists of a PC that receives message data from the user and a direct digital synthesizer (DDS) that generates the voltage signal. It also includes a power amplifier and a loop antenna to form the magnetic field signal, as shown in Figure 2.

The DDS (AD9854) is a signal generator that follows the process in Figure 3. The DDS initially receives message data in the form of ASCII characters from the control software on the PC. The delimiter 'ÿ', signifying the end of a message, is inserted after the message data. This message set is converted to ASCII binary data and encoded with the Manchester code, which is a self-clocking signal with no DC component to facilitate synchronization with the receiver. The OOK modulated signal pertaining to the processed binary data is then generated. The carrier frequency for modulation is set to 60kHz to maximize the magnetic field-to-voltage conversion ratio of the GMI sensor, as found in the literature [8].

The modulated signal is conveyed to a power amplifier (AR, 75A400) to maximize the transmission power for a more extended communication distance. The amplified signal is

TABLE 1. Geometrical parameters of the loop antenna.

Turns	Inner diameter of coil [mm]	Outer diameter of coil [mm]	Copper wire strands	Copper wire diameter [mm]
10	110	250	600	0.12

TABLE 2. Electrical parameters of the loop antenna.

Self - inductance [μH]	Matching capacitance [nF]	Parasitic resistance [mOhm]	Resonance frequency [kHz]
21.93	315	47.63	60

fed into the antenna. To transmit the magnetic field signal, we fabricated a loop antenna in the form of a flat spiral coil with Teflon-coated Litz wire for waterproof functions in an underwater or humid environment. The design parameters of the loop antenna are listed in Table 1. The transmitter coil is designed as an LC-series resonant circuit to form a stronger magnetic field through a high coil current. This resonance topology can maximize the current flowing through the antenna by canceling the reactance of the circuit at the frequency point of electrical resonance. The relevant electrical parameters of the loop antenna are listed in Table 2. With minimized impedance from resonance, the flowing current I of the coil is maximized to 770mA. When X_L is the reactance of the coil without a matching capacitor, the AC reactive power of the coil can be approximately 5W, which is calculated by I^2X_L [12]. From the measurement result of the input impedance (Z_{11}) with a vector network analyzer (Agilent, E5071C), the antenna input impedance at the target resonance frequency of 60kHz is $-26.4\text{dB}\Omega$.

Although the resonance state removes the reactance, the parasitic resistance of 47.63 mΩ still exists. The resistance component of the coil determines the quality factor (Q-factor), referring to the concentration of the energy at resonance: $Q = X_L/R$. When the resistance of the coil is increased by the introduction of parasitic resistance from the coil structure, the Q-factor is decreased, and the transmitting efficiency is decreased according to the low concentration of the energy at resonance. However, this resistance component can support better communication performance because the Q-factor is reversely proportional to the bandwidth, meaning that the resistance component contributes to increasing the bandwidth. Because the channel capacity is proportional to the bandwidth, a wide bandwidth contributes to a high data rate. The bandwidth of the fabricated antenna is 337.5Hz. Although the bandwidth value is not wide enough to match the bandwidth of a commercialized communication system, the transmitter adopts the single frequency of 60kHz which is the carrier frequency in OOK modulation; hence, the bandwidth of an antenna is sufficient to cover the transmitting signal.

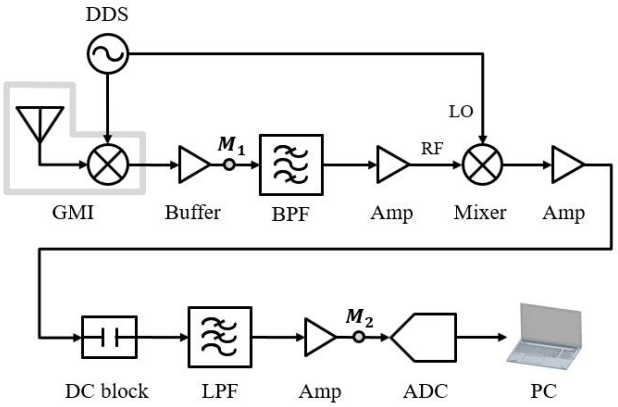

FIGURE 4. Schematic of the receiver system composed of a GMI sensor and a demodulator. The converted digital data after the ADC are transmitted to a PC to be processed.

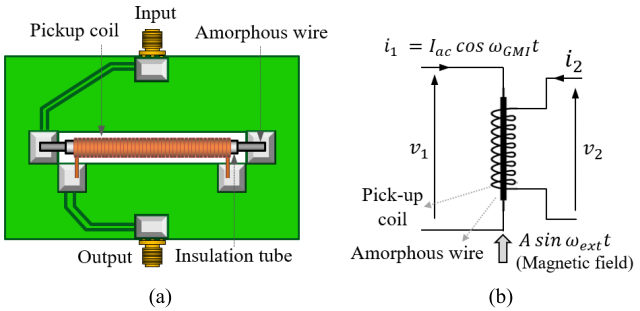

FIGURE 5. GMI sensor composed of the amorphous wire, pick-up coil and insulation tube: (a) schematic view, and (b) sensing schematic in the form of a two-port network.

TABLE 3. Design parameters of the GMI sensor.

GMI wire diameter [μm]	GMI wire length [mm]	Pick-up coil turns	Pick-up coil length [mm]	Overall PCB size [mm^3]
100	85	750	75	95

B. RECEIVER SYSTEM

The receiver system consists of a GMI sensor that receives the external magnetic field signal, a demodulating circuit, and a PC to acquire and process the digital signal, as shown in Figure 4.

The first stage of the receiver system is the GMI sensor, which receives the external magnetic field. The sensing element is composed of a thin pick-up coil wound directly on a CoFeSiB-based amorphous wire mounted in the middle of a printed circuit board (PCB), as illustrated in Figure 5(a) [13]. The design parameters of the GMI sensor are listed in Table 3. As shown in Figure 5(b), the GMI sensor can be modeled as a two-port network. When the external magnetic field reaches the amorphous wire in a parallel direction, a high variation of the off-diagonal impedance in the amorphous wire is generated. The off-diagonal impedance, identical to the transfer impedance from the amorphous wire to the pick-up coil, is utilized to improve the noise performance in the

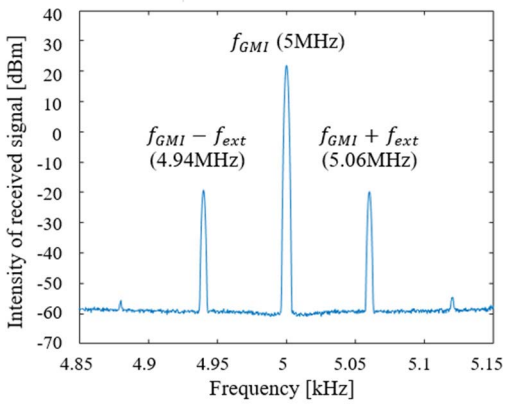

FIGURE 6. Spectrum of the received signal which is measured at the output of the GMI sensor. The received signal is composed of 3 kinds of frequencies according to superheterodyne topology of the sensor.

proposed structure [14]. Here, the intrinsic impedance of the pick-up coil forms the noise voltage with the current i_2 flowing through the coil in the GMI sensor. In order to obtain the integrity of the output signal, the noise generated from intrinsic impedance should be suppressed. This issue can be solved by deploying a voltage buffer after the sensor because the current i_2 becomes zero. As a result, the power loss from this intrinsic noise is minimized and improved sensitivity can be achieved.

The DDS (Keysight, 33500B) in the receiver system excites the driving current i_1 to the GMI sensor at f_{GMI}. The voltage signal v_2 at the pick-up coil terminals is induced by the current i_1 flowing through the amorphous wire and the change in off-diagonal impedances according to the external magnetic field. During this progress, the frequency of the voltage signal is identical to that in the result of AM modulation of the frequency of the external magnetic field and driving current with the superheterodyne topology of the GMI sensor. The detailed proof of frequency components is given by [7, eq. (1)-(2)]. Under the condition in which the frequencies of the external magnetic field and driving current are correspondingly f_{ext} and f_{GMI}, the frequencies of the voltage signal are composed of $f_{GMI} + f_{ext}$, $f_{GMI} - f_{ext}$, f_{GMI}. The spectrum of the received signal is measured by a spectrum analyzer (Keysight, N9000B) as shown in Figure 6. Here, we set f_{GMI} to 5MHz according to the measurement result of the off-diagonal impedance of the GMI sensor with the voltage buffer. The highest value of impedance is shown up near 5MHz. Accordingly, we considered 5MHz as the optimal frequency to obtain the best sensitivity for this configuration. In the case of f_{ext}, we found the optimal value of 60kHz to show the highest MVCR through sweeping the carrier frequency in earlier work [8]. Moreover, SFDR can be sustained over 35dBc when f_{ext} is set to 60kHz. A bandpass filter (BPF) screens out undesirable signal components such as intermodulation frequencies and un-eliminated intrinsic noise from the peripherals and sensors. Through the BPF, the voltage signal only composed of $f_{GMI} + f_{ext}$ is extracted.

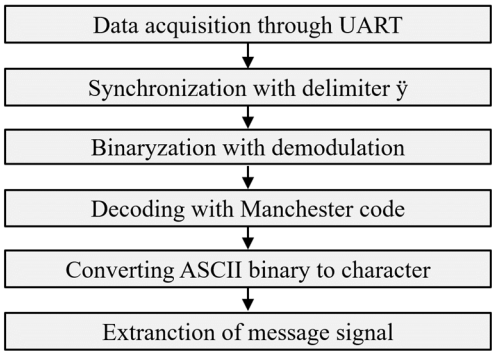

FIGURE 7. Procedure of signal processing of digital data on the PC.

This voltage signal does not undergo flicker noise due to the fact that the magnetic field signal in kHz is up-converted to $f_{ext} + f_{GMI}$ in MHz. The noise immunity from these structures makes the GMI sensor the most promising candidate among receivers for magnetic field communications. The amplifier compensates for the loss of the filter and amplifies the voltage signal of $f_{ext} + f_{GMI}$. This signal is separated into a signal of a frequency of f_{ext} through the process of demodulation by a down-mixer. The mixer receives the signal at the frequency of f_{GMI} from the DDS as a local oscillator and down-converts the modulated signal of $f_{ext} + f_{GMI}$. This results in the extraction of a signal of f_{ext} identical to the frequency of the external magnetic field.

Subsequently, the process to increase the resolution of the extracted signal in the form of OOK is implemented. The amplifier increases the signal intensity. The direct current (DC) block cuts off the low-frequency components near 0Hz. The low-pass filter (LPF) removes the components above 100kHz to obtain the f_{ext} signal clearly. The amplifier again compensates for the loss of the two processes of filtering and conveys the signal to an analog-to-digital converter (ADC, ATmega128). The converted digital data is transmitted to the PC through UART communication for further demodulation and decoding.

Although the acquired data on the PC is digital data, this is still in the OOK modulation form. An envelope detector is generally used to demodulate the OOK waveform on an incoherent system. Here, demodulation in this system is implemented by the signal processing software. The use of the envelope detector results in the voltage drop because of the diode in the detector. This voltage drop limits the detection range; hence, we decide to realize the OOK demodulation through signal processing software instead of using the envelope detector.

The procedure of the signal processing, including demodulation, is shown in Figure 7. As mentioned in the description of the transmitter system, the message data generated by the PC and DDS has the delimiter 'ÿ' at the endpoint of the message. The message data consist of strings entered by a user in a repeated form. In order to interpret the data in the receiver system, the confirmation of the starting point of the message data is necessary beforehand. The digital data transmitted

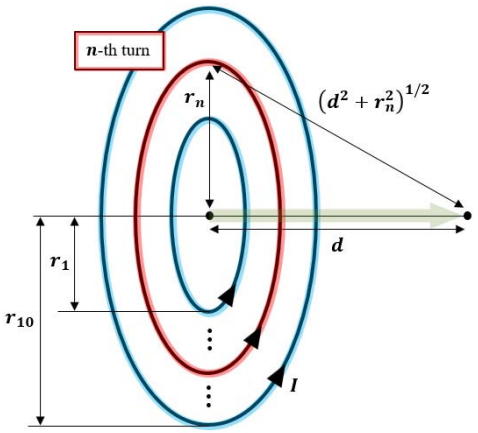

FIGURE 8. Schematic design of the loop antenna at the transmitter and the propagation of the magnetic field to a direction perpendicular of the loop.

through UART is initially synchronized with the delimiter 'ÿ' independently generated by the receiver software. This delimiter is also digital data OOK-modulated with a 60kHz sinusoidal carrier and expresses ASCII binary data of 'ÿ' encoded with the Manchester code. Cross-correlation of the message data and delimiter is conducted to identify the end of the message data. Although the message data can be partly distorted, the result of cross-correlation at the location of the delimiter has the highest value. Therefore, the start and end of the message data can be recognized.

The synchronized data are demodulated and become binary data via the following process. First, the mean of each bit amplitude is calculated. The receiver system knows the data rate and sampling rate; the receiver system is also aware of the number of data points in one bit. According to the start point identified by synchronization and the bit length information, calculating the amplitude mean of each bit is repeatedly performed by iteratively shifting to the next bit. The bit corresponding to logic '0' has a mean value that converges to zero or to a small value, while the bit for logic '1' has a much higher mean value than zero. Here, the optimal threshold to distinguish the logic '1' and '0' is selected from the median between the highest amplitude of '0' and the lowest amplitude of '1'. This operation minimizes the possibility of misclassifying logic '1' and '0' during the following step. If the value exceeds the threshold, the bit data '1' will be added to the last position of the resulting array, and vice versa. The demodulation and binarization of the data are then completed with the binary data array. The extracted binary data is decoded by the Manchester code and converted to ASCII characters. By removing the delimiter ÿ, the message data can be completely restored in the receiver system.

III. CHANNEL EVALUATION

When a time-varying current flows through the loop antenna at the transmitter system, a magnetic field carrying the data information is generated based on Faraday's law. The magnetic field used for communication is near-field communication at several hundreds of meters at 60kHz. With the non-radiative characteristic of the near field, magnetic field communication takes advantage of multipath propagation and the low absorption of the signal from the lossy medium, which can be a critical problem for conventional wireless communication through EM waves [15]. Although these communication issues are negligible in magnetic field communication, the skin effect generated by the eddy current from the time-varying magnetic field can limit the performance of the communication range. The skin depth δ is the location at which the propagating signal attenuates by a factor of 1/e. For good conductors, the skin depth is expressed as $\delta = 1/\sqrt{\pi f \mu \sigma}$, where ω is the angular frequency, μ is the permeability, ϵ is the permittivity, and σ is the electrical conductivity. However, communication with poor conductor media such as seawater and soil must apply the more general expressions of the skin depth via the following expression [16].

$$\delta = \left[\omega\sqrt{\frac{\mu\epsilon}{2}}\left(\sqrt{1+\left(\frac{\sigma}{\omega\epsilon}\right)^2}-1\right)\right]^{-1} \tag{1}$$

Path loss of magnetic field signal can be predicted according to four parameters in the skin depth expression. The channel model based on a mathematical expression is used in order to analyze the magnetic field communication channel. The magnetic field generated by the loop antenna can be modeled with the following description. As explained in Section II-A, the fabricated loop antenna is a flat-spiral coil with ten turns. According to Maxwell's equations, the magnetic field formed from the loop from which uniform sinusoidal current $Icos(\omega t)$ flows can be expressed as follows [16]:

$$\begin{aligned} H_\theta &= \frac{j\omega\mu m\gamma^2}{4\pi\eta}\left[\frac{1}{\gamma R}+\frac{1}{(\gamma R)^2}-\frac{1}{(\gamma R)^3}\right] sin(\theta)e^{-\gamma R} \\ H_\phi &= 0 \\ H_r &= \frac{j\omega\mu m\gamma^2}{2\pi\eta}\left[\frac{1}{(\gamma R)^2}+\frac{1}{(\gamma R)^3}\right]\cos(\theta)e^{-\gamma R} \end{aligned} \tag{2}$$

where m is the magnetic moment, γ is the propagation constant, η is the intrinsic impedance. R is the vector of the loop edge to the measurement point, and the magnitude of R is $\sqrt{(r^2+d^2)}$ where r is the radius of the loop and d is the distance from the center of the loop to the measurement point. In the near-field region, the magnitude of γR is less than 1. Therefore, the term $1/(\gamma R)^3$ is only considered, and the other terms $1/(\gamma R)$ and $1/(\gamma R)^2$ are negligible. Because we assume that the measurement point is aligned with the center of the loop, θ is 0 and H_θ then converges to 0. The magnetic moment m is expressed as $NI\pi r^2$, where N is the turns of the loop. Considering the dimension and structure of the fabricated coil, the radius r for the nth turn can be expressed as $r_n = 0.0515 + 0.007n$. By multiplying the permeability μ, we can

TABLE 4. Electrical properties of media environments.

	Air	Water	Sand	Soil	Saline water1	Saline water2
Conductivity [mS/cm]	0	0.001	1	10	40	80
Relative permeability	1	0.999	1.002	1	0.999	0.999
Relative permittivity	1.001	81	3.75	5.1	81	81

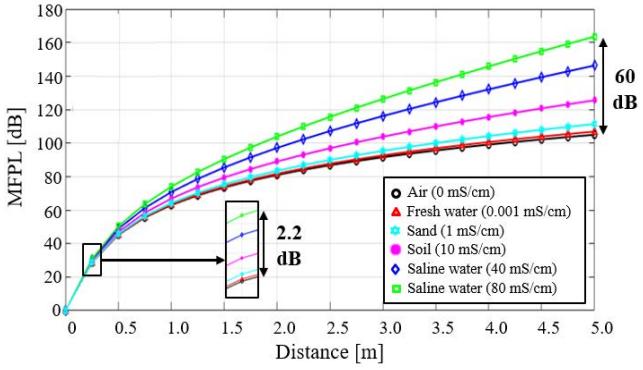

FIGURE 9. Magnetic field path loss (MFPL) as a function of the distance.

define the magnetic flux density as follows:

$$B_{total} = \sum_{n=1}^{10} \frac{Ir_n^2}{2\left(1+\frac{\sigma}{j\omega\epsilon}\right)^{1/2}(d^2+r_n^2)^{3/2}} e^{-j\frac{(d^2+r_n^2)^{1/2}}{\delta}} \quad (3)$$

where δ is the skin depth. The schematic design of the loop antenna and magnetic field propagation is illustrated in Figure 8. Equation (3) can be converted to the expression of magnetic field path loss (MFPL) on the dB scale with the following equation:

$$\text{MFPL} = -20\log\frac{B_{total}(d)}{B_{total}(0)} \quad (4)$$

Here, equation (4) only considers the magnitude, omitting the direction component because we assume a single straight direction. With (4), the loss of the magnetic field signal can be predicted, presenting insight with regard to an extension of the communication range. The concept of MFPL was introduced in the literature [6].

The communication media used for the measurements consist of air, fresh water, saline water, dry soil, and sand. The saline water is 40mS/cm, similar to general seawater, and saline water of 80mS/cm is used to identify the impact of conductivity on the magnetic field. The material properties of the media are listed in Table 4 [17]–[20]. Figure 9 depicts the MFPL as a function of the distance for the given material properties. The trend of MFPL shows that the electrical conductivity of the media strongly affects the magnetic field channel. For distances shorter than 1m, the overall figures

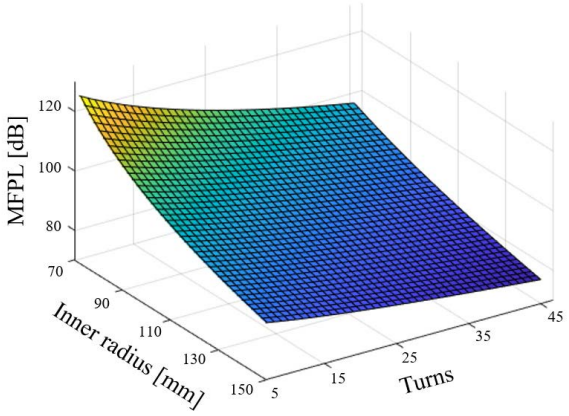

FIGURE 10. Magnetic field path loss as a function of the radius and number of turns of the loop antenna at the transmitter.

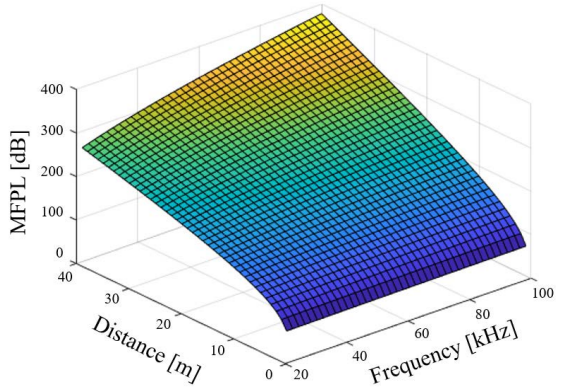

FIGURE 11. Magnetic field path loss as a function of the distance and frequency of the current flowing through the loop antenna at the transmitter.

are on a similar level; however, a greater gap between the figures arises as the distance becomes longer. Despite the fact that the magnetic field communication overcomes EM challenges such as multipath fading and the radical loss from the properties of the media, deterioration of the communication performance according to the conductivity of the media should be considered when designing the system.

In conductive channel environments, generating a stronger magnetic field is one method by which to lengthen the communication distance. Antenna parameters such as the radius and number of turns must be adjusted to ensure the high intensity of the field. Figure 10 shows the MFPL with the radius and the turns of the transmitting antenna. Here, it is assumed that the medium is air and the communication distance is 10m. As expected from the fact that larger size and more turns contribute to the magnetic moment, the MFPL becomes lower with an increase in the radius and number of turns. Moreover, we can predict that the frequency of the magnetic field can serve as a factor to lower the MFPL because the loss generated from the eddy current is greatly dependent upon the frequency. Figure 11 shows the MFPL with the frequency of the field and distance. The dimensions

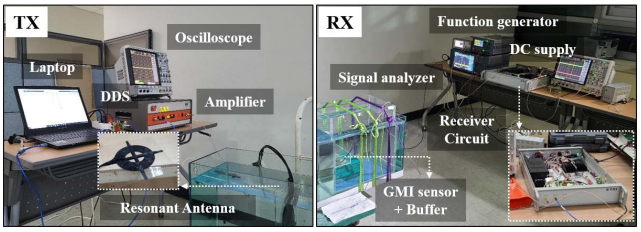

FIGURE 12. Experimental setup of the transmitter and receiver system to evaluate the communication performance.

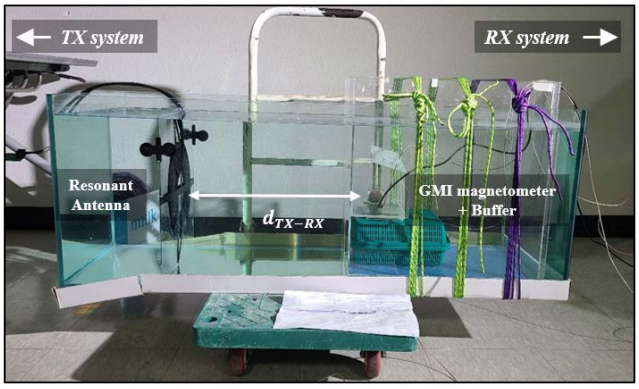

FIGURE 13. Experimental setup of magnetic field channel using container to evaluate communication with media condition.

TABLE 5. System configurations.

Parameter	Value
Current flowing the antenna	770mA
AC reactive power	5W
Carrier frequency	60kHz
Data rate	100bps
GMI driving voltage	6V
GMI driving voltage offset	1.3V
GMI driving frequency	5MHz

of the coil follow the fabricated design. The MFPL tends to become higher with an increase in frequency, and this transition is greater with a longer distance. From this result, we find that the use of a high frequency for field carriers can critically affect the communication performance; hence, a low frequency is desired to lower the eddy loss. However, we have to consider the target data rate and optimal condition of the GMI sensor. The carrier frequency of the modulated signal should be obtained to ensure a sufficient data rate. This means that lowering the frequency to reduce MFPL can limit the data rate of the system. On the one hand, the GMI sensor fabricated has the optimal frequency condition for the reception of the magnetic field. From a previous study [8], the carrier frequency of 60kHz is the optimal frequency to obtain the largest MVCR of the GMI sensor. Therefore, the frequency setting should be assessed considering not only the MFPL but also the target data rate. This tradeoff between frequency selection and communication performance needs to be considered in terms of the entire system design.

The performance when receiving the magnetic field signal can be limited by the noise characteristics of the media environments and the sensitivity of the GMI sensor. In practical environments such as those that are underground and underwater, the magnetic field is exposed to various forms of background noise that disrupt communication. This type of noise is mainly composed of low-frequency components generated from living organisms, artificial devices, earth resonance, and other sources [21]. As explained in Section II, the GMI sensor has a superheterodyne topology that can overcome the limitation of the aforementioned low-frequency noises generated from various channel environments. The sensitivity of the GMI sensor can be obtained by dividing the noise power spectral density (N-PSD) into the MVCR; it was measured as 52.1pT/$\sqrt{Hz}$ in a previous study [8]. Based on equation (3) and the media condition, the communication distance recognizable by the GMI sensor can be approximately predicted as follows: 9.3m in air, 8.2m in fresh water, 6.6m in sand, 4.5m in soil, 3.3m in saline water of 40mS/cm, and 2.7m in saline water of 80mS/cm. These estimates are solely based on the reception performance of the GMI sensor. In the receiver system overall, including the sensor and demodulation circuit, the reception performance for the magnetic field signal can be worse than in the case of a sole GMI sensor according to the electrical characteristics of various circuit components.

IV. MEASUREMENT SCENARIOS AND ANALYSIS METHODS

Experiments are conducted to verify the performance of the communication system using the GMI sensor. In earlier work [8], we mainly measured and analyzed the electrical characteristics of the GMI sensor, in that case the MVCR, SFDR, and N-PSD, to identify the feasibility of communication with the GMI sensor as a receiver antenna. Here, we evaluate the performance of the receiver system in terms of the BER, SFDR, and random noise. The experimental setup for magnetic field communication by the proposed transmitter and receiver system is configured as shown in Figure 12. A small-scale communication system in the near range is constructed and utilized to take the measurements. In Figure 13, The line of sight is aligned to the center of the transmitter antenna and the amorphous wire of the GMI sensor and stretched by interval distance d_{TX-RX}. This interval distance can be extended maximally up to 1m which is four times the outer diameter of the antenna at the transmitter system. The antenna and the container surrounding the GMI sensor are completely immersed in the media to reflect the effect of the material properties.

For wireless sensor networks which utilize magnetic field communication, maintaining the stable operation against a noisy environment and accurate signal transmission regardless of channel media condition is the key point to achieve the high performance system. In this study, we limit the communication range to 1m to more focus on the stability with the low-noise characteristic and reliability with the low-error

system to verify the applicability of the system in the practical environment. We use a much lower scale of power to transmit the magnetic field signal than the power generated from the conventional transmitter. As we mentioned in Section III, the communication distance over 1m is theoretically achievable based on the high sensitivity of the GMI sensor. Moreover, adopting the higher power of transmitter will be able to expand the communication range. Even though we confine the communication distance within 1m, it does not mean extending the distance is not achievable. This will be the topic of our further works with optimal transmitter design and improved system.

The system configurations of the transmitter and receiver system are listed in Table 5. With minimized impedance from the resonant state of the loop antenna in the transmitter system, the flowing current I of the coil is 770mA and the AC reactive power of the coil can be approximately 5W. The GMI sensor has an optimal driving voltage of 6V. Moreover, the driving voltage offset is set to 1.3V to ensure high sensitivity and low noise performance considering the characteristics of the ferromagnetic material. By introducing the offset voltage, the sensor can maintain a low level of coercivity, which is related to the sensing resolution, and low Barkhausen noise generated from the movement of the magnetic domain according to the external magnetic field [22], [23]. As Section II mentioned, The GMI driving frequency is set to 5MHz according to the measurement result for off-diagonal impedance as a function of the driving frequency.

The analysis methodologies of the receiver performance are as follows. First, the intensity of the received signal at the sensor output at M_1 in Figure 4 is measured to analyze path loss as a function of the communication distance with different media conditions. Based on the output of the sensor, we analyze noise characteristics as well. The SFDR is the dynamic range between the fundamental signals and the highest spurious signal components, corresponding to the highest noise in the spectrum. A larger SFDR results in a lower probability of being affected by noise when the fundamental signal is measured. We identify that the highest noise from the sensor is the second harmonic ($f_{GMI} + 2f_{ext}$) of the fundamental signal ($f_{GMI} + f_{ext}$) according to the signal analyzer. Hence, the SFDR can be considered as the difference in the intensity between the fundamental signal and the second harmonic. The second harmonic is one of the major components contributing to the distortion of the signal in a non-coherent demodulation system. Therefore, the measurement of the SFDR must be done in order to analyze the noise characteristic according to the communication distance and media.

Second, the peak stability of the signal at M_2 in Figure 4 is measured to analyze the effects of random noise from the noise sources surrounding the receiver. Random noise is mainly generated from the thermal noise of the electronic device and the intrinsic noise of the electronic component. The OOK-modulated waveform affected by random noise has the non-uniform carrier waveform filling a square wave, referring to a data bit. This results in misclassification of the bit logic during the demodulation process. Accordingly, the demodulation and decoding of the message data remain incomplete, and the BER will increase dramatically. In order to analyze the effects of random noise, the standard deviation of the voltage peak values for logic '1' during the unit interval is measured at the point before the ADC. More precisely, the subject to be measured is the voltage peak of the waveform of a 60kHz sinusoidal wave, filling the square wave as logic '1'. Greater deviation means that the system is more exposed to random noise interference. In other words, the receiver deals with a low-quality signal. Comparing cases with different conditions can provide insight into the communication performance in the presence of noise.

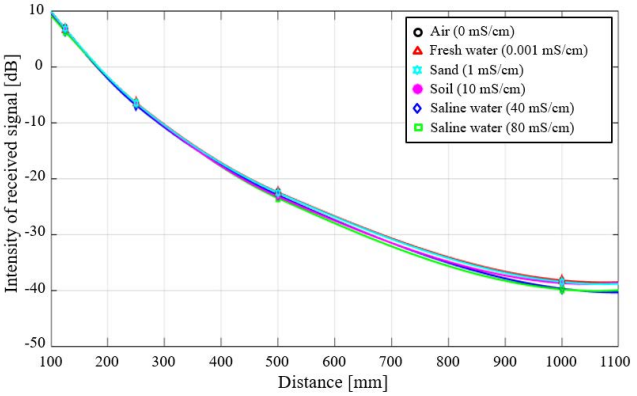

FIGURE 14. Output of the GMI sensor as a function of the distance. This signal is utilized when calculating the SFDR as the fundamental signal.

Third, the BER of the received signal is measured to compare the ideal communication environments. By comparing the measurement results with simulation results and theory-based estimations, the adequacy of the proposed system compared to the ideal system can be verified. Furthermore, the BER as a function of the distance is measured to identify the impact of an increase in the distance on the performance of the receiver. A BER analysis offers insight into communication distances with the maximum allowable bit error considering the receiver system overall. In this measurement, the signal intensity can be too strong to recognize the trend of the BER. Therefore, BER measurements with noise artificially added to the data are also conducted to assume low-intensity signaling and high-noise environments.

V. RESULTS

As introduced in Section IV, we measured the intensity of received signal through the output of the GMI sensor under the transmission distance conditions of 125, 250, 500, and 1000mm as shown in Figure 14. These results show the propagation aspects of the magnetic field under diverse conditions, referring to the intensity of the signal. The tendency of an increase in path loss with the distance is identical to the MFPL estimates in Section III. The path loss difference according to the media conditions is negligible due to the

TABLE 6. Standard deviation and mean of the demodulated signal before ADC.

Distance	Air		Water		Sand		Soil		Saline water (40 mS/cm)		Saline water (80 mS/cm)	
	μ [V]	σ	μ [V]	σ	μ [V]	σ	μ [V]	σ	μ [V]	σ	μ [V]	σ
125mm	5.054	0.088	5.057	0.087	5.055	0.088	5.063	0.091	5.048	0.088	5.054	0.091
250mm	4.826	0.172	4.617	0.146	4.726	0.159	4.641	0.144	4.499	0.156	4.377	0.163
500mm	2.319	0.216	2.331	0.230	2.295	0.236	2.159	0.213	2.262	0.241	2.173	0.201
1000mm	0.347	0.201	0.340	0.186	0.331	0.196	0.329	0.188	0.339	0.193	0.316	0.192

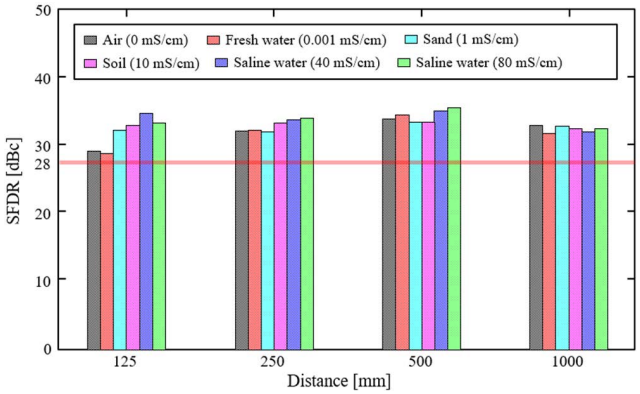

FIGURE 15. Measurement result for the SFDR of the received signal.

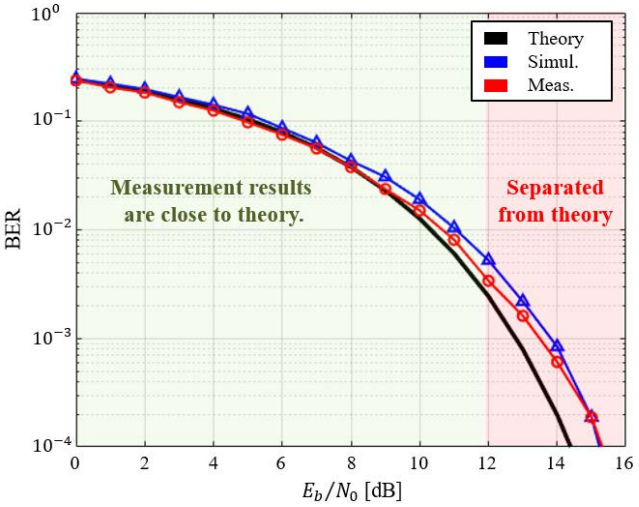

FIGURE 16. Comparison of BER performance outcomes for non-coherent OOK.

short communication distance of less than 1m. Although some part of the eddy current loss is likely to be omitted due to the limitation of the small-scale prototype system, the overall tendency of a received signal is identical to calculated estimates in Figure 9; hence, the measurement results are meaningful. Through these measurement results, we can infer that the magnetic field is applicable to the communication with nearly constant performance despite the different media conditions.

Figure 15 shows the measurement result for the SFDR of the received signal. The SFDR in all cases exceeds 28dBc, showing that the media and distance conditions scarcely affect the performance of the GMI sensor. Considering that the SFDR remains at a similar level despite the change in the distance, the noise impact on the fundamental signal is indistinguishable according to a signal attenuation over longer distances because power reduction with longer distance applies not only fundamental signal but also noise components. The performance of the GMI sensor, according to the electrical conductivity of the media, also remains on a similar level. The result showing a high-SFDR means that the received signal is much higher than not only the second harmonic but also the noise floor. Therefore, we can predict that the signal intensity in this setup is high enough to avoid the impact of the random noise, which is measured on the noise floor.

The signal at M_2 in Figure 4 is the result of demodulation through the GMI sensor and signal conditioning with analog components, in this case the filter, amplifier, and mixer. Table 6 shows the mean (μ) and standard deviation (σ) of the signal at M_2 during the unit interval (0.01sec). As listed in the table, the standard deviation is lower than 0.1 at 125mm due to the saturated output of the amplifier and remains near 0.2 regardless of the distance except for the cases of 125mm. It was found that the impact of noise is independent of the power reduction of the signal with increases in the distance. Also, the receiver system, which includes a demodulation circuit, can keep the level of the standard deviation of the peak voltage similar regardless of the media condition. Considering a standard deviation near 0.2, random noise arises at a very low level, meaning that the noise level of the signal in the system is very low.

A BER analysis is implemented with several measurements. The comparison of BER for the theory, simulation, and measurement results is conducted with 500mm of air as the default state. The theoretical equation of BER for non-coherent OOK is

$$P_b \cong \frac{1}{2}\left\{1+\frac{1}{\sqrt{2\pi E_b/N_0}}\right\}e^{-\frac{1}{2}E_b/N_0} \cong \frac{1}{2}e^{-\frac{1}{2}E_b/N_0} \quad (5)$$

under the condition of $E_b/N_0 \gg 1$, where E_b is the average bit energy and N_0 is the noise power spectral density under additive white Gaussian noise [24]. As shown in Figure 16,

TABLE 7. BER as a function of the communication range.

	Air	Water	Sand	Soil	Saline water (40mS/cm)	Saline water (80mS/cm)
125mm	0	0	0	0	0	0
250mm	0	0	0	0	0	0
500mm	0	0	0	0	0	0
1000mm	0	0	6.25e-6	6.25e-5	0	2.5e-5

the trends in the results remain similar up to AWGN with SNR of 12dB. The trends after 12dB of E_b/N_0 show that the results of the simulation and measurements begin to diverge from the estimates based on theory. In contrast to the theory-based BER performance assuming the ideal system, the other results from simulation and measurements have finite-amplitude conditions and exposure to diverse noise sources such as intrinsic noise of the electronic components and ferromagnetic core [23]. When E_b/N_0 is lower than 12 dB, the AWGN is strong enough to cover the impact of the other noise. However, when E_b/N_0 is over 12 dB, the AWGN is so weak that the BER performance gets directly affected by the other noise. Nonetheless, the trends for all cases sustain a similar tendency. From this result, the receiver system is capable of sufficient performance close to ideal OOK communication in BER. Considering the measurement of the SFDR and standard deviation of the voltage peak, the intensity of the received signal, which corresponds to E_b, is much higher than the level of the noise floor, consisting of random noise. The random noise in this system, corresponding to N_0, exists at a very low level. This means that E_b/N_0 in Figure 16 exists at a very high level. Therefore, we can infer that BER without AWGN in practical measurements will likely converge to zero.

The measurement result of BER as a function of the communication range and media condition without AWGN is listed in Table 7. As predicted, the BER results of all cases converge to a very low value with the fabricated system setup, meaning that the proposed system is capable of high communication performance despite the power reduction of the received signal at greater distances. However, these BER figures can stem from the much higher intensity of the received signal compared to that of the noise components. Accordingly, a noise impact and deterioration of the communication performance are not found due to the close distance or the overpowered signal from the transmitter.

In order to analyze the BER trends when the received signal is weaker than the original signal, AWGN for SNR of 12dB is artificially added to the received digital signal. The figure of 12dB is identical to the point that theoretical BER for the ideal non-coherent OOK begins to diverge from the BER measurements, as shown in Figure 16. When adding an error by AWGN, the BER recognizably increases with the communication distance in a general system, as illustrated in Figure 17. This indicates that the proposed communication

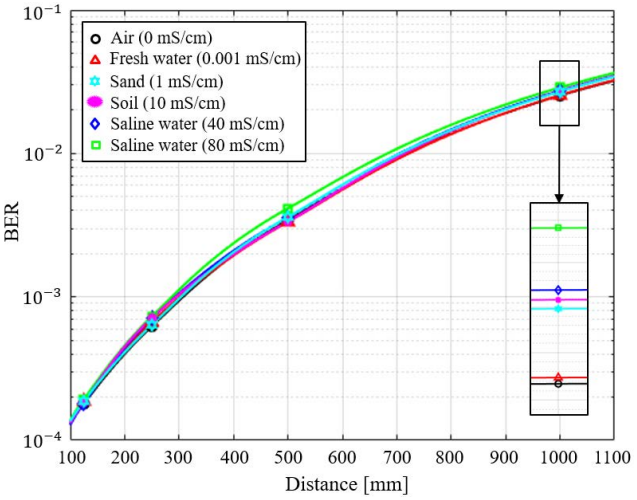

FIGURE 17. BER as a function of the communication range with AWGN (SNR = 12 dB).

system is proven to operate properly as a general communication system in diverse channel environments. Also, the order of BER for the proposed system according to the type of media is aligned with the electrical conductivity, as estimated with the magnetic field model in the form of MFPL.

VI. CONCLUSION

In order to check the feasibility of a GMI sensor as a magnetic field receiver, several studies were conducted [7], [8]. Following previous research, this paper introduced a magnetic field communication system that relies on a GMI sensor as a field receiver. The communication with a specific transmission distance was designed with the LC-series resonant antenna to achieve high transmission efficiency in the transmitter system, which we had not realized in previous research. Based on its high sensitivity and immunity against low-frequency noise, the GMI sensor can receive a magnetic field signal transmitted 1m away from the transmitter. The channel environments tested here consist of air, water, saline water, soil, and sand. These were used to identify the variation of the communication performance according to the electrical conductivity of the medium.

The paper verified the applicability of the GMI sensor-based communication system in the practical environment through an experimental demonstration with different communication distances and channel media conditions, which had not been proposed. The proposed system showed low interference from the second harmonic and random noise in the received signal according to corresponding measurements of the SFDR and peak stability of the modulated waveform. Furthermore, the BER performance of the system is close to that of an ideal system based on theory up to AWGN for SNR of 12dB. With these results, a low value of BER can be theoretically inferred and practically proven to be true at the following BER measurement. The BER performance with AWGN for SNR of 12dB was also measured to assume low-intensity signaling and high-noise environments.

These measurements proved that the proposed system can achieve excellent communication performance and that it is applicable as a practical system in RF-challenged environments. Besides, this result shows the possibility of the proposed system to realize improving wireless communication in EM shadow areas and proposes the direction of the magnetic field communication system with a methodology adopting the high-sensitivity magnetometer.

This study fabricated a communication system as a prototype with a communication range of 1m. Although we artificially added an error to the signal to mimic a power reduction, actual communication with a longer distance from the transmitter to the receiver is likely to be different from the measurement results presented in this paper. For further works, research to achieve a broader communication range needs to be conducted for a detailed analysis of the impact of a conductive medium and noisy environment. To realize the wider range, the design of the transmitter antenna should be improved to cover a longer line of sight by optimizing the antenna structure, and adopting the higher power of the transmitter should be considered. In addition, this study lacks an analysis of the power and cost of the whole system. To build up the improved system in the future, we should cover a comprehensive analysis to consider the power and cost of the system. Furthermore, different modulation schemes such as frequency shift keying (FSK) and phase shift keying (PSK) can be tried to achieve low BER and low power consumption in future works. The data rate of 100bps is also the limitation of this study; hence, the work to get a higher data rate is needed to apply to the conventional communication application. Therefore, there are still many steps to achieve the improvement of the system, and it is highly required to conduct in future works.

The GMI sensor-based magnetic field communication system proposed in this study is proven to have applicability in the practical environment through a series of experiments. This communication system will be core technology in the field demanding high-performance magnetic field communication based on its stability and reliability. It is predicted that the proposed system will be utilized in the field of WSN applications in RF-challenge environments such as monitoring natural disasters and maintaining artificial facilities in remote areas where data collection by humans would be difficult such as underwater or underground environments. In the case of using a short communication range, the proposed system is also available with high-sensitivity characteristics. For example, the microrobot inserted in the human body can adopt this system because the micro-scale of the magnetic field signal can be used to communicate and minimize the impact of the magnetic field on humans. This can be achievable because of the portability and availability of minimization of the GMI sensor with keeping the high sensitivity. The proposed experiment methodology will also be used to verify the system adopting the GMI-sensor in related research. The proposed system and experimental verification will elevate the level of magnetic field communication and show the possibility of advancing the conventional system in the future.

ACKNOWLEDGMENT

(Seunghun Ryu and Kibeom Kim are co-first authors.)

REFERENCES

[1] Z. Sun and I. F. Akyildiz, "Magnetic induction communications for wireless underground sensor networks," *IEEE Trans. Antennas Propag.*, vol. 58, no. 7, pp. 2426–2435, Jul. 2010.
[2] J. Lee, H. J. Lee, J.-Y. Kim, and I.-K. Cho, "Gaped two-loop antenna-based magnetic transceiver with an empirical model for wireless underground communication," *IEEE Access*, vol. 9, pp. 34962–34974, 2021.
[3] M. C. Domingo, "Magnetic induction for underwater wireless communication networks," *IEEE Trans. Antennas Propag.*, vol. 60, no. 6, pp. 2929–2939, Jun. 2012.
[4] V. Gerginov, F. C. S. da Silva, and D. Howe, "Prospects for magnetic field communications and location using quantum sensors," *Rev. Sci. Instrum.*, vol. 88, no. 12, Dec. 2017, Art. no. 125005.
[5] M. Hott, P. A. Hoeher, and S. F. Reinecke, "Magnetic communication using high-sensitivity magnetic field detectors," *Sensors*, vol. 19, no. 15, p. 3415, Aug. 2019.
[6] M. Hott and P. A. Hoeher, "Underwater communication employing high-sensitive magnetic field detectors," *IEEE Access*, vol. 8, pp. 177385–177394, 2020.
[7] J.-Y. Kim, I.-K. Cho, H. J. Lee, J. Lee, J.-I. Moon, S.-M. Kim, S.-W. Kim, S. Ahn, and K. Kim, "A novel experimental approach to the applicability of high-sensitivity giant magneto-impedance sensors in magnetic field communication," *IEEE Access*, vol. 8, pp. 193091–193101, 2020.
[8] K. Kim, S. Ryu, J.-Y. Kim, I.-K. Cho, H.-J. Lee, J. Lee, and S. Ahn, "Giant magnetoimpedance receiver with a double-superheterodyne topology for magnetic communication," *IEEE Access*, vol. 9, pp. 82903–82908, 2021.
[9] D. Murzin, D. J. Mapps, K. Levada, V. Belyaev, A. Omelyanchik, L. Panina, and V. Rodionova, "Ultrasensitive magnetic field sensors for biomedical applications," *Sensors*, vol. 20, no. 6, p. 1569, Mar. 2020.
[10] R. A. Seymour, N. Alexander, S. Mellor, G. C. O'Neill, T. M. Tierney, G. R. Barnes, and E. A. Maguire, "Interference suppression techniques for OPM-based MEG: Opportunities and challenges," *NeuroImage*, vol. 247, Feb. 2022, Art. no. 118834.
[11] A. L. Herrera-May, L. A. Aguilera-Cortés, P. J. García-Ramírez, and E. Manjarrez, "Resonant magnetic field sensors based on MEMS technology," *Sensors*, vol. 9, no. 10, pp. 7785–7813, Sep. 2009.
[12] M. Ceraolo and D. Poil, *Fundamentals of Electric Power Engineering: From Electromagnetics to Power Systems*, 1st ed. Hoboken, NJ, USA: Wiley, 2014.
[13] B. Dufay, S. Saez, C. P. Dolabdjian, A. Yelon, and D. Menard, "Characterization of an optimized off-diagonal GMI-based magnetometer," *IEEE Sensors J.*, vol. 13, no. 1, pp. 379–388, Jan. 2013.
[14] B. Dufay, S. Saez, C. Dolabdjian, A. Yelon, and D. Ménard, "Impact of electronic conditioning on the noise performance of a two-port network giant magnetoimpedance magnetometer," *IEEE Sensors J.*, vol. 11, no. 6, pp. 1317–1324, Jun. 2011.
[15] I. F. Akyildiz, P. Wang, and Z. Sun, "Realizing underwater communication through magnetic induction," *IEEE Commun. Mag.*, vol. 53, no. 11, pp. 42–48, Nov. 2015.
[16] D. K. Cheng, *Field and Wave Electromagnetics*, 2nd ed. Boston, MA, USA: Reading, MA, USA: Addison-Wesley, 1989.
[17] J. H. Scott, "Electrical and magnetic properties of rock and soil," Dept. Interior, U.S. Geol. Surv., Washington, DC, USA, Open-File Rep. 83-915, 1966.
[18] W. E. Patitz, B. C. Brock, and E. G. Powell, "Measurement of dielectric and magnetic properties of soil," Sandia Nat. Lab., Albuquerque, NM, USA, Tech. Rep. SAND95-2419, 1995. [Online]. Available: https://www.inis.iaea.org
[19] T. Katsube, R. A. Klassen, Y. Das, R. Ernst, T. Calvert, G. Cross, J. Hunter, M. Best, R. DiLabio, and S. Connell, "Prediction and validation of soil electromagnetic characteristics for application in landmine detection," *Proc. SPIE*, vol. 5089, pp. 1219–1230, Sep. 2003.
[20] J. Rhebergen, H. Lensen, P. Schwering, G. Marin, and J. Hendrickx, "Soil moisture distribution around land mines and the effect on relative permittivity," *Proc. SPIE*, vol. 4742, pp. 269–280, Aug. 2002.

[21] M. Muzzammil, N. Ahmed, G. Qiao, I. Ullah, and L. Wan, "Fundamentals and advancements of magnetic-field communication for underwater wireless sensor networks," *IEEE Trans. Antennas Propag.*, vol. 68, no. 11, pp. 7555–7570, Nov. 2020.
[22] D. Jiles, *Introduction to Magnetism and Magnetic Materials*, 2nd ed. Ames, IA, USA: Chapman & Hall, 1998.
[23] B. D. Cullity and C. D. Graham, *Introduction to Magnetic Materials*, 2nd ed. New York, NY, USA: Wiley, 2009.
[24] F. Xiong, *Digital Modulation Techniques*, 2nd ed. Boston, MA, USA: Artech House, 2006.

SEUNGHUN RYU received the B.S. degree from Koreatech, Cheonan, South Korea, in 2020, and the M.S. degree from The Cho Chun Shik Graduate School for Green Transportation, Korea Advanced Institute of Science and Technology (KAIST), Daejeon, South Korea, in 2022. His research interests include the magnetic field communication, signal integrity analysis and design for high-speed interconnection, and electromagnetic interference (EMI).

KIBEOM KIM received the B.S. degree from Koreatech, Cheonan, South Korea, in 2011, and the M.S. and Ph.D. degrees from the Korea Advanced Institute of Science and Technology (KAIST), Daejeon, South Korea, in 2014 and 2019, respectively. His current research interests include electromagnetic interference/electromagnetic compatibility for three-dimensional integrated circuits packages and magnetic sensors.

JANG-YEOL KIM received the B.S., M.S., and Ph.D. degrees in information and communication engineering from Chungbuk National University, Cheongju, Republic of Korea, in 2010, 2012, and 2017, respectively. Since 2012, he has been with the Electronics Telecommunications Research Institute, Daejeon, Republic of Korea. His research interests include antenna design, thermal therapy algorithms, microwave sensing, and electromagnetic sensors.

IN-KUI CHO received the B.S. and M.S. degrees from the Department of Electronic Engineering, Kyungpook National University, Daegu, South Korea, in 1997 and 1999, respectively, and the Ph.D. degree in electrical engineering from the Korea Advanced Institute of Science and Technology, Daejeon, South Korea, in 2007. Since May 1999, he has been with the Electronics and Telecommunications Research Institute, Daejeon, where he has designed and developed optical backplane, optical chip-to-chip interconnect system, and magnetic resonance wireless power transfer. His current research interests include simulation and development of WPT components, such as planar magnetic resonators and magnetic resonators for three-dimensional WPT.

HAERIM KIM received the M.S. degree from The Cho Chun Shik Graduate School of Green Transportation, Korea Advanced Institute of Science and Technology (KAIST), Daejeon, South Korea, in 2019, where she is currently pursuing the Ph.D. degree. Her current research interests include the wireless power transfer system design and electromagnetic interference (EMI) and electromagnetic field (EMF).

JANGYONG AHN received the M.S. degree from The CCS Graduate School for Green Transportation, Korea Advanced Institute of Science and Technology (KAIST), South Korea, in 2018, where he is currently pursuing the Ph.D. degree. His research interests include electromagnetic interference/electromagnetic compatibility (EMI/EMC) and human exposure to EMF from wireless power transfer systems.

JUNSUNG CHOI (Member, IEEE) received the B.S., M.S., and Ph.D. degrees in electrical and computer programming engineering from Virginia Tech, in 2013, 2016, and 2018, respectively. He is currently a Research Professor with the Center for Green Transportation System, KAIST, Daejeon, South Korea. His research interests include vehicular communications, V2X communications, propagation channel characteristics, 5G communications, and LPI communications.

SEUNGYOUNG AHN (Senior Member, IEEE) received the B.S., M.S., and Ph.D. degrees from the Korea Advanced Institute of Science and Technology, Daejeon, South Korea, in 1998, 2000, and 2005, respectively, all in electrical engineering. From 2005 to 2009, he worked as a Senior Engineer at Samsung Electronics, Suwon, South Korea, where he was in-charge of high-speed board design for laptop computer systems. He is currently a Professor with The Cho Chun Shik Graduate School of Green Transportation, Korea Advanced Institute of Science and Technology. His research interests include wireless power transfer system design and electromagnetic compatibility design for electric vehicles and high-performance digital systems.